Enhancing the AC network stability with a grid-forming control for single-stage PV inverter

Jaume Girona-Badia, Vinícius A. Lacerda, Eduardo Prieto-Araujo, Oriol Gomis-Bellmunt
CITCEA-UPC
jaume.girona@upc.edu

***Index Terms*—Grid-forming, PV, Renewable Energy Resources, Solar Generation**

***Abstract*—This article proposes a PLL-less grid-forming (GFor) control for a PV central power plant topology designed to maintain the DC voltage and improve the AC voltage stability. The PV single-stage or central topology stands as the most widely adopted power plant structure. However, no GFor control capable of regulating the DC bus has yet been proposed for this layout. This work presents a PLL-less GFor control that can effectively control the DC voltage for a single-stage PV inverter, whether it operates at the Maximum Power Point (MPP) or with reserve. Moreover, this control can incorporate Maximum Power Point Tracking (MPPT) controls typically employed in grid-following structures. The primary advantage of this GFor control is the voltage support and stability it provides and the capability of working with a low Short Circuit Ratio (SCR). The performance and viability of the proposed control was analyzed with several simulations of various faults (symmetrical and asymmetrical), frequency (large phase jump and frequency excursion with high ROCOF) and resource events (irradiation changes and DC voltage reference tracking analysis). The results demonstrate that the proposed GFor control presented not only meets the grid-code requirements but also exhibits the behaviour expected during the different analyzed events.**

I. Introduction

The increasing penetration of renewable energy sources has led to a reduction in the number of Synchronous Generators (SG) in the AC networks, resulting in a decrease in the inertia, voltage stability and short-circuit current [1]. Among the existing solutions to overcome such issues, the use of grid-forming (GFor) controls for the Voltage Source Converters (VSCs) is becoming the preferred choice. The GFor can improve the stability of AC networks thanks to its voltage-source behaviour, enabling the integration of higher levels of renewable energy sources into electrical power systems, such as the solar farms [2]–[4].

The GFor converters can support the grid in different ways, such as improving the AC voltage stability, emulating virtual inertia or providing fast frequency response (rapid provision of power reserve due to a frequency excursion) [4]. The provision of fast frequency response and inertia depends on the resource limitations [5]. If no additional storage is implemented, the energy reserve of the converter is limited to the DC-link capacitor [5]. Moreover, to supply a fast frequency response, the converter must operate below the Maximum Power Point (MPP). However, this power provision will be limited by resource availability. Nevertheless, the GFor control will still be capable of providing voltage support and voltage stability to the system.

The GFor functionalities that the PV power plant will be able to provide will also depend on the PV topology. There are three main PV power plant connection topologies: the central, the string and the multistring [6]–[10] . The central (single-stage) topology uses one converter to connect all the PV panels. This converter will regulate the DC voltage and the AC power injection. The string structure implements one DC-AC converter for each string, and the different converters are connected in parallel in the AC network. The multistring architecture employs a DC-DC converter for each string and a single DC-AC converter to connect to the grid. The multistring and the string topologies allow for a more precise Maximum Power Point Tracking (MPPT) and the AC-DC converter's DC voltage is decoupled from the generated power. The central topology is the most used in large PV plants, due to its lower cost in the inverters and its feasibility [7], [8], but the power generated by the PV will depend on the AC-DC converter's DC voltage.

Different approaches have been considered in the literature to apply the GFor control to PV sources. In [11], a GFor control is implemented to a PV source with a DC/DC converter. This control adds a droop with a parallel PI for the voltage to avoid exceeding the MPP voltage. Other studies consider operating the PV in grid-following and having another converter in parallel operating in GFor, which has a battery or a supercapacitor [12], [13]. In [14], [15], GFor unique structures have been presented for PV generation. In these cases, a DC/DC converter is always used. A control for the PV single stage is proposed in [16]. Nevertheless, the DC voltage is not directly controlled, and the control is not tested during faults or large ROCOFs, that may discharge the DC bus. To the best of the authors' knowledge, no GFor control has been proposed for the central (single-stage) topology, with DC voltage control, which is needed to ensure the voltage level during transients.

Aiming to address these challenges, this manuscript will provide the following principal contributions:

- A PLL-less GFor control for a central topology PV power plant that controls the DC bus voltage, without the need for additional storage or DC/DC converter, is presented.
- Analysis on the robustness of the control with AC network events such as of phase jumps, high ROCOFs and faults.

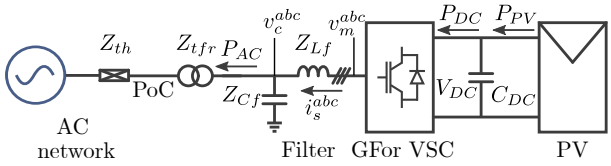

Fig. 1. PV single-stage scheme.

- Analysis on the effect of variation of resource power production.
- An analysis of the limitations of the PV single-stage GFor operation.

The remainder of this paper is organized as follows. Section II presents the problem description. The control proposed for the PV single-stage inverter is described in Section III. In Section IV, different dynamic simulations are carried out to validate the control presented. Finally, the conclusions are summarized in Section V.

II. Problem Description

This section will present the main problems of implementing a GFor in a central PV power plant. The system is depicted in Fig. 1. There, it can be observed that there is only one converter in the system, which needs to operate in GFor whereas regulates the DC voltage. Thus, implementing the grid-forming in a single-stage PV source has a primary challenge: controlling the DC bus while it operates in grid-forming.

The voltage support and stability are the main pillars of the GFor and the control must be able to provide them in all operation modes. However, the provision of power during frequency events is also desired. To provide this power, the PV power plant needs to have a power or energy reserve. To have a power reserve, the DC voltage needs to be bigger than the MPP voltage. Then, the DC voltage needs to be controlled and the control strategy needs to be able to set a DC voltage reference. However, this DC voltage is not desired to be constant. In the event of a frequency decrease, the DC voltage must decrease to supply the frequency reserve. Conversely, when the PV plant is operated at MPPT or its reserve is fully provided, precise DC voltage control is required while ensuring the GFor operation.

The GFor implemented in a PV single-stage must also accomplish the grid-code requirements. Not disconnecting in certain transients such as faults, frequency excursions or phase jumps. The control must be designed to affront these cases and meet the grid-code requirements.

III. Control

This section describes the GFor control implemented to the central PV power plant converter. The control is divided into 4 parts: synchronization loop, voltage control, current limiter and current controller (see Fig. 2). The voltage and current are controlled in both positive and negative sequences [17], [18].

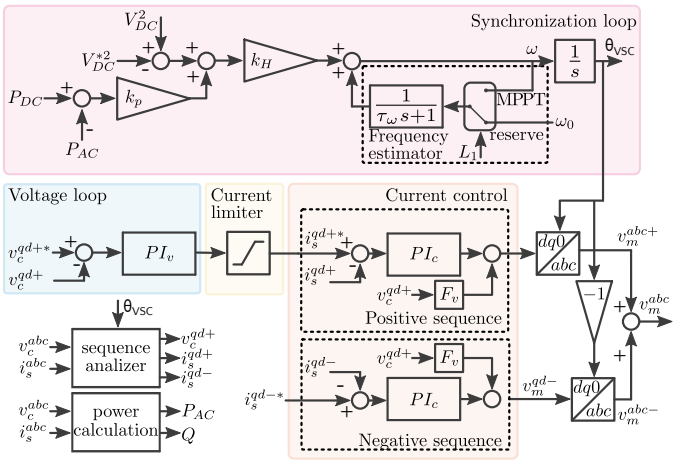

Fig. 2. Grid-forming control for single stage PV

A. Synchronitzation loop

The synchronization loop sets the converter's phase. In this case, the proposed PLL-less control focuses on directly regulating the DC voltage and indirectly controlling the active power. The control has two operation modes: with a power reserve and implementing an MPPT control. Each operation mode uses a different frequency estimator, as shown in Fig. 2. Moreover, distinct DC voltage references are employed in each mode. The operational mode (L_1) can be manually selected. However, when set to operate with reserve and either the power reserve is depleted or a fault occurs, it automatically switches to MPPT operation mode.

1) With reserve: The frequency estimator is set to a constant value equal to the system's base frequency and the DC voltage reference is set to the desired voltage (over the MPP voltage). The control equation in this operation mode is:

$$\omega = \omega_0 + k_H \left(V_{DC}^2 - V_{DC}^{*2} + k_p (P_{DC} - P_{AC}) \right), \quad (1)$$

where ω and ω_0 are the frequency imposed by the converter and the system's base frequency, respectively, k_H is the inertia parameter, V_{DC} and V_{DC}^* are the DC voltage and its reference respectively, k_p is the damping parameter, P_{AC} is the active power injected into the AC system and P_{DC} is the sum of the DC power from the PV panel and the capacitor (see Fig. 1). If the system is in steady state P_{AC} and P_{DC} will be equal, then in steady state the following relation is found:

$$\omega - \omega_0 = k_H \left(V_{DC}^2 - V_{DC}^{*2} \right) \quad (2)$$

As can be seen in (2), k_H will relate the frequency with the voltage. If the frequency decreases, the voltage will decrease, increasing the power injected into the grid due to the PV voltage-power relation. Then, to tune the k_H parameter, the following strategy is employed:

$$k_H = \frac{m_p (P_{DC}^{MPP} - P_{DC}^{reserve})}{V_{DC}^{reserve} - V_{DC}^{MPP}} \quad (3)$$

where m_p is the desired static frequency-power droop frequency response that is usually set by the TSO, $P_{DC}^{reserve}$

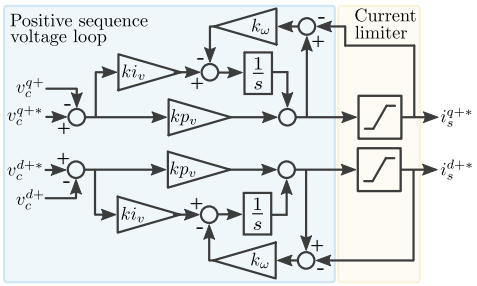

Fig. 3. Voltage control for single stage PV

is the power exchange operating with reserve, P_{DC}^{MPP} is the maximum power available, V_{DC}^{MPP} is the MPP DC voltage and $V_{DC}^{reserve}$ is the DC voltage that provides the $P_{DC}^{reserve}$.

2) MPPT: When the reserve is depleted, or the converter is operated at the MPP, thanks to an MPPT control. The frequency estimator [19]–[22] is set to the converter's frequency filtered in this operation. Notice that the filter is always in use to smooth the transition between operations. This change affects the control's dynamics.

Equation (2) is reformulated taking into account the frequency estimator change:

$$\omega \frac{\tau_\omega s}{\tau_\omega s + 1} = k_H \left(V_{DC}^2 - V_{DC}^{*2} \right), \tag{4}$$

where τ_ω is the frequency filter time constant. In the steady state, the frequency estimated and the converter frequency will match. Then, from (4), it can be deduced that $V_{DC} = V_{DC}^*$ in steady state. This control mode can track the DC voltage reference with precision. Then, the DC voltage reference (V_{DC}^*) has to be set at the value that extracts the maximum power from the PV. To find this value, the same MPPT controls implemented in grid-following converters can be used. However, it should be noted that this control will not inject inertia or any frequency response since no power or energy reserve is left.

B. Voltage loop

The voltage loop is only implemented in the positive sequence. As it can be seen in Fig. 3, the control is composed of two PI controllers. Moreover, an anti-windup is applied to the integral part. This structure is similar to the one implemented in [18].

C. Current limitation

The strategy applied in this control is prioritizing the positive sequence's reactive power during faults. To do it, the current limiter prioritizes the q component of the positive sequence. When the current is limited, the synchronization loop is configured in MPPT operation mode, and the DC voltage references to a voltage that provides 0 active power ($V_{DC}^* = V_{DC}^{P0}$). Then, during faults, when the current is limited, the converter will provide reactive power but not active power. The negative sequence current is always set to 0.

TABLE I
SYSTEM PARAMETERS

Parameter	Symbol	Value	Units
AC network			
Short Circuit Ratio	SCR	1,5-5	
	R_{th}/L_{th}	1/10	
Nominal voltage	U_{nom}	33	kV
Frequency	f	50	Hz
PV power plant			
Nominal Power	P_{nom}	4.2	MVA
Nominal voltage	U_{nom}	33	kV
Frequency	f	50	Hz
Maximum current	I_{max}	1.2	pu
DC capacitance	C	103.7	mF
DC minimum voltage	V_{DC}^{min}	900	V
DC maximum voltage	V_{DC}^{max}	1500	V
Filter inductance	L_{Lf}	0.1	pu
	R_{Lf}/L_{Lf}	1/20	
Filter capacitance	C_{Cf}	0.1	pu
Filter capacitance's resistance	R_{Cf}	0.005	pu
Transformer inductance	L_{trf}	0.1	pu
Transformer resistance	R_{trf}	0.01	pu
Control parameters			
Voltage PI control	PI_v	$\frac{s+650}{s}$	pu
Current PI control	PI_c	$\frac{0.63662s+10}{s}$	pu
Voltage feed-forward filter	F_v	$\frac{1}{0.001s+1}$	
Inertia parameter	k_H	8.2684 e-6	pu
Damping parameter	k_p	0.4523	pu

D. Current control

The current control is applied in the positive sequence and in the negative sequence. Both sequences share the same structure. Each sequence implements two PI controllers and a filtered feed-forward [23]. However, the decoupling is not implemented since when both sequences are used, the decoupling branches are cancelled [24].

IV. SIMULATIONS

This section presents various simulation results to show the performance and stability of the GFor control presented. Moreover, the viability of operating a central PV power plant in GFor is analyzed. Also, the modulation of the PV panels is explained.

The simulations are carried out in MATLAB®Simulink. The system analyzed is depicted in Fig. 1, whose main parameters can be found in Table I, the tuning design implemented is obtained from [25]. The AC network has been represented as an ideal voltage source behind an impedance. Two short circuit ratios, 1.5 and 5, have been used to demonstrate that the control is capable of working with low SCRs. The incidents analysed can be divided into three groups: faults, AC network frequency and resource events.

The converter parameters are based on the Power Electronics Freesun HEM EIC solar converter [26], which is modelled using an average model [27].

A. PV panels modelling

The PV panels have been modelled using the single-diode model [28]. This model presents a good compromise between

TABLE II
PV PANEL PARAMETERS, BASED ON JA SOLAR®JAM72S30-545/MR.

V_{oc} (V)	49.75
V_{DC}^{MPP} (V)	41.80
i_{DC}^{MPP} (A)	13.04
i_{sc} (A)	13.93
β_V_{oc} (%/ºC)	-0.275
α_I_{sc} (%/ºC)	+0.045

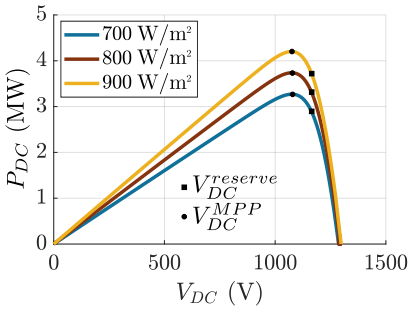

Fig. 4. PV operational points.

simplicity and precision [29]. The panel uses the parameters from Table II, based on the JA SOLAR®JAM72S30-545/MR.

The PV park is composed of 325 parallel lines of 27 PV panels in series to obtain the desired voltage and power. The distinct operational points of the conjunction of PV panels are shown in Fig. 4 and Table III. Notice that the power injected operating in reserve is 90 % of the maximum power available ($P_{DC}^{reserve} = 0.9P_{DC}^{MPP}$). Further, it can be seen that the voltage variation of V_{DC}^{MPP} and $V_{DC}^{reserve}$ for the different irradiation levels is unnoticeable.

The central topology analyzed implements a VSC to convert the power from DC to AC and control the PV power plant. The parameters of this converter are defined in Table I.

B. Faults

Two faults have been applied at the Point of Connection (PoC) operating with reserve mode. First, a three-phase-to-ground fault is simulated to analyze the capability to manage the active power during an event. Second, a two-phase-to-ground fault is applied to show the capability of controlling the negative sequence current. In all cases, the fault resistance is 0 and the fault duration is 250 ms.

In Fig. 5, the simulation of the three-phase-to-ground fault is shown. The voltage is highly reduced due to the fault. However, the voltage is restored in a few milliseconds after the fault is dissipated. The positive sequence current is increased, prioritizing the component q (the reactive power injected is low because the fault is close to the converter, and the current is limited to 1.2 pu). The negative sequence is maintained at 0. During the fault, the active power is set to 0, prioritizing the injection of reactive power. To achieve this, the DC voltage is adjusted to V_{DC}^{P0} and set to MPPT operation mode, reducing the power extracted from the PV panels during the fault. After the fault, the active power is restored in less than half a second thanks to the synchronizing control DC voltage control capabilities. When the fault is extinct, the DC voltage is set again to the $V_{DC}^{reserve}$. The frequency is controlled during the fault and restored after the fault in less than a quarter of a second. Overall, the fault capability with SCR 1.5 and 5 accomplishes the grid-codes requirements (see Fig. 7), prioritizing the injection of reactive power.

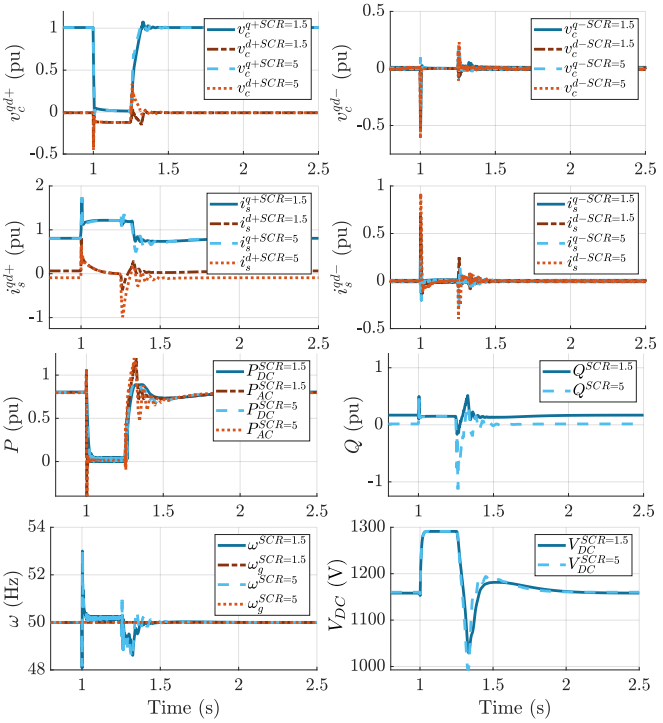

Fig. 5. Three-phase-to-ground fault performance of the control proposed.

Fig. 6 depicts the main parameters of the system during a two-phase-to-ground fault with low SCRs (1.5 and 5). The positive sequence voltage is reduced during the fault. Moreover, the negative sequence voltage is not zero due to the asymmetric fault. However, the negative current is still controlled to 0, and the i_s^{q+} is prioritised. The DC voltage is set to V_{DC}^{P0} during the fault to limit the active power exchanged. The active and reactive power oscillates at 100 Hz during the asymmetrical fault due to the disequilibrium caused by the fault. The operation is recovered in less than 250 ms when the fault is cleared. As it can be seen in Fig 7, the control during the fault with both SCRs accomplishes the grid-codes' voltage requirements. Moreover, the negative sequence current is controlled to 0, even though it is not instantaneous.

TABLE III
PV OPERATIONAL POINTS.

Irradiation (W/m²)	**700**	**800**	**900**
$V_{DC}^{reserve}$ (V)	1160	1160.5	1160.3
$P_{DC}^{reserve}$ (MW)	2.943	3.3638	3.78
V_{DC}^{MPP} (V)	1074.8	1073.2	1073
P_{DC}^{MPP} (MW)	3.27	3.7375	4.2

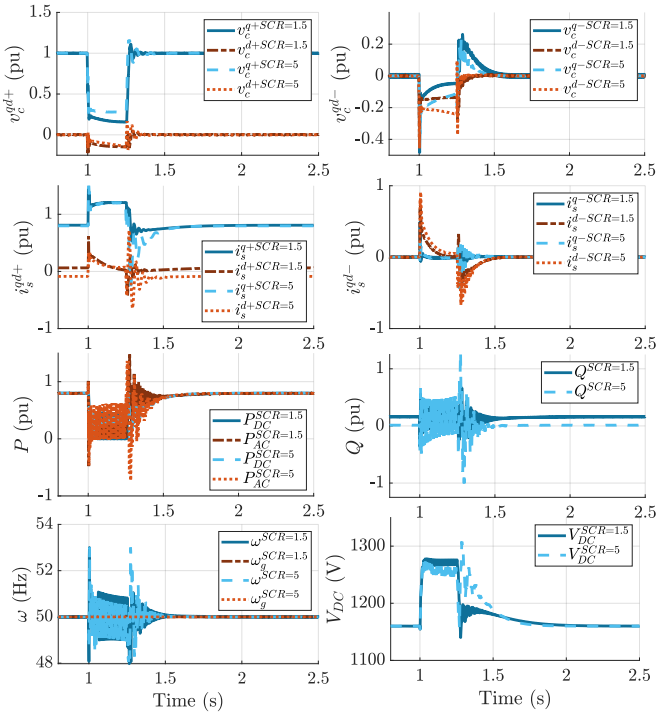

Fig. 6. Two-phase-to-ground fault performance of the control proposed.

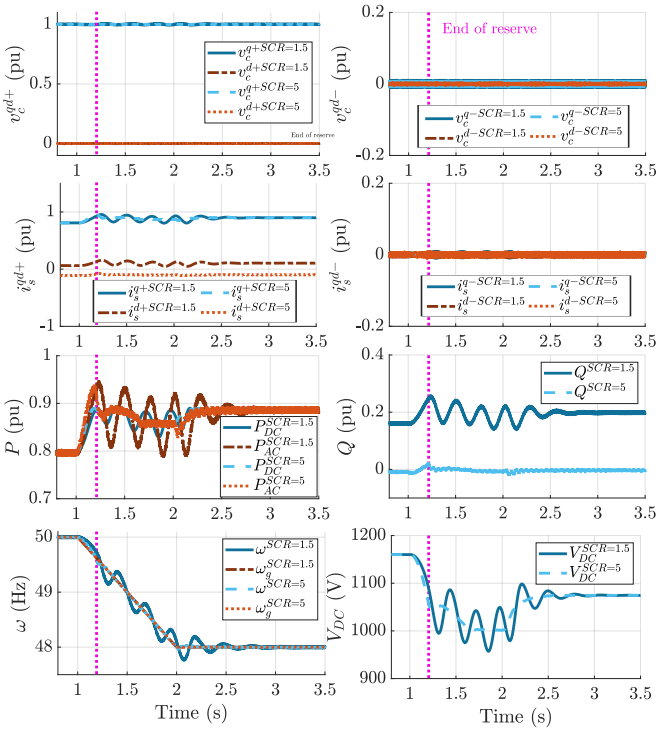

Fig. 8. ROCOF performance of the control proposed.

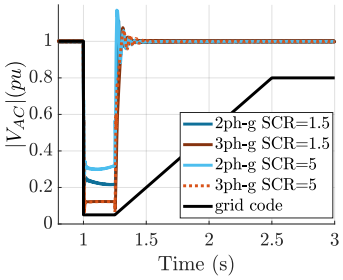

Fig. 7. AC voltage for the analyzed faults compared with the grid-code requirements.

The voltage during faults meets the grid-codes fault-right-through requirements [30] in all cases, as shown in Fig. 7. In conclusion, the control is capable of maintaining operation and fulfilling the requirements during a fault.

C. AC network frequency events

The frequency events simulated are i) a frequency excursion with a ROCOF of 2 Hz/s for 1 s and ii) a 10 ° phase jump in the AC grid. These two events serve to illustrate the frequency behaviour of the converter. Moreover, the provision of inertia and frequency response is analysed, highlighting their limits.

Figure 8 illustrates the principal parameters of the system during a frequency deviation with a large ROCOF. There, it can be seen that the AC voltage is well-controlled, with no relevant variations observed during this event. In contrast, the current exhibits minor oscillations during the event when the SCR is 1.5, which are generated by the change of operation due to the total provision of reserve. These fluctuations are also reflected in the frequency, active and reactive power and DC voltage. However, these oscillations do not lead to an unstable system and only manifest during the period of high ROCOF (once the frequency is constant again, they vanish). However, if the SCR is 5, they are unnoticeable.

The control effectively provides the power reserve during the frequency event. Moreover, since the power reserve is completely supplied (marked in Fig. 8 with a magenta line), the control operation transitions from the with reserve to the MPPT operation. The DC voltage is maintained in between the converter limits during the transient, thanks to the DC voltage-oriented synchronization control. Finally, it can be noticed that not only is the power reserve provided, but the energy stored in the capacitor is also partially provided (emulated as inertia). This is the reason why the injected power into the AC network (P_{AC}) exceeds the power extracted from the PV panels (P_{DC}) during the transient. In conclusion, the control is stable during the frequency excursion with a large ROCOF, providing the frequency response desired while regulating the AC voltage.

The 10º phase jump event is illustrated in Fig. 9. There, it can be seen that when the SCR is 5, more oscillations appear than when the SCR is 1.5. However, these fluctuations are dissipated in less than 100 ms. As desired in GFor, the power increases when the event occurs, leading to a discharge of the DC capacitor due to its low energy storage. Two different behaviours depending on the SCR can be found. When the SCR is 1.5, the voltage is reduced, but it is over the V_{DC}^{MPP} (see table III), which increases the power delivered by the PV panels ($P_{DC}^{SCR=5}$) providing more power. If the SCR is 5, the DC voltage drops below the V_{DC}^{MPP}, decreasing the

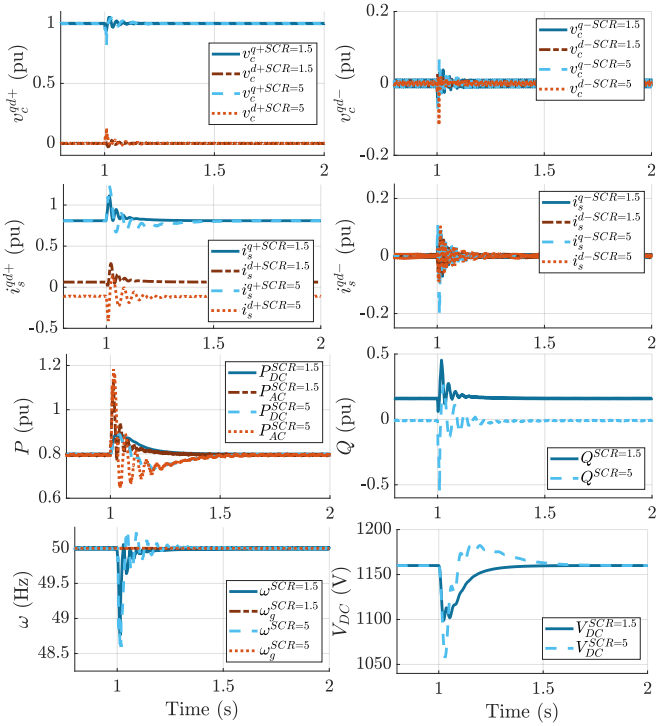

Fig. 9. 10º phase jump performance of the control proposed.

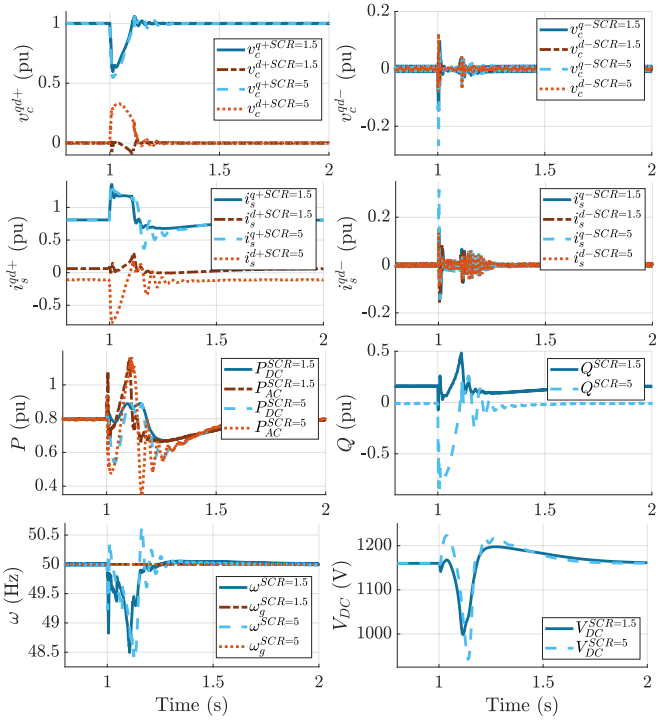

Fig. 10. 30º phase jump performance of the control proposed.

power delivered in the first instant of the event. Even though the voltage is below the V_{DC}^{MPP}, the system is stable due to the synchronization control implemented (Section III-A). However, the behaviour in the case of having an SCR equal to 1.5 is more desirable due to the fewer oscillations and the more power provided. Nevertheless, after the event, the converter resynchronizes with the AC network and the same steady state as before the event is reached in both cases.

Figure 10 depicts a 30º phase jump event. When the phase jump is 30º, both SCR cases achieve the V_{DC}^{MPP}. Consequently, the operation is changed to MPPT mode to limit the DC voltage decrease. In this scenario, the transient is more severe than the 10º phase jump event. However, the converter does not exceed its current and voltage limits, and the transient is dissipated within 0.2 seconds for both cases. This simulation demonstrates the control capability of sustaining the stable operation even in the presence of large phase jumps.

D. Resource events

Three resource events are simulated: i) an irradiation instantaneous variation, operating with reserve, ii) an irradiation instantaneous change, operating in MPPT, and iii) voltage reference increase when the converter operates in MPPT mode. These events show how the control behaves when the resource is not constant. Furthermore, the tracking of the DC voltage is demonstrated. The different PV operational points analysed are defined in Fig. 4 and Table III.

In Fig. 11, the irradiation variation event operating the converter with reserve (Section III-A1) is presented. In both SCRs, the event is similar. The radiation decrease reduces the DC power generated. Thus, this lack of power discharges the DC bus, which obliges the synchronization loop to reduce injection power into the AC network to maintain the same DC voltage ($V_{DC}^{reserve}$). The transient ends in less than 600 ms. After the transient, the voltage is at the same level. However, the power injected into the AC has decreased due to the irradiation reduction. When the radiation rises, the behaviour is the opposite. The DC voltage increases and the synchronization control injects more power into the AC network. In both cases, the V_{DC} is in between the limits.

Notice that in both cases, the $V_{DC}^{reserve}$ is more or less the same value with different radiations, see Table III and Fig. 4, meaning that the power delivered after the event is near the 90 % of the available power. However, the V_{DC}^{*} can be changed to have a power reserve of exactly 10 % of the power available.

Figure 12 shows a variation in the radiation while functioning in MPPT mode. The behaviour is similar to the case with reserve. However, some oscillations appear, mainly in the case of SCR = 5. Nevertheless, the synchronization control is capable of controlling the DC voltage after the transient, exchanging power into the AC network. The new operational point is not the MPP. If the new MPP is desired, the V_{DC}^{*} has to be changed to the new V_{DC}^{MPP} (which can be done using an MPPT).

The results of a step jump in the DC voltage reference (V_{DC}^{*}), from 1074.6 V to 1100 V, implementing the MPPT operation, are plotted in Fig. 13. As can be seen, the control can perform a perfect tracking of the DC voltage. This ensures that MPPT techniques used in grid-following controls can

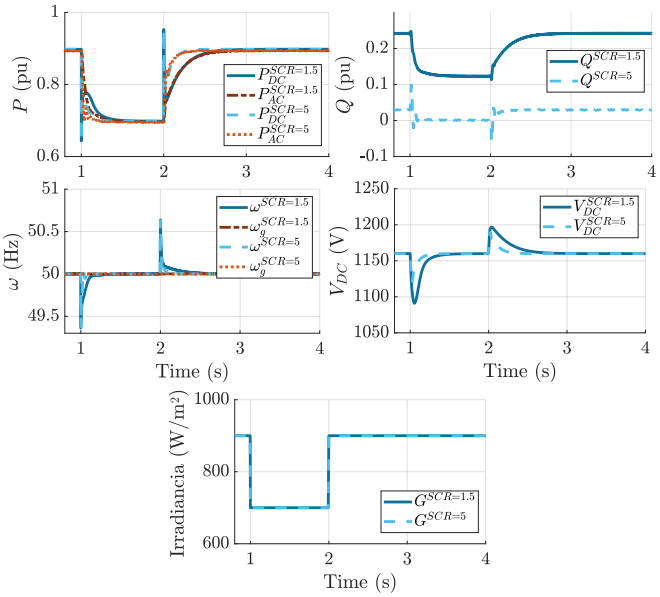

Fig. 11. Irradiation step performance of the control proposed, operating with reserve mode.

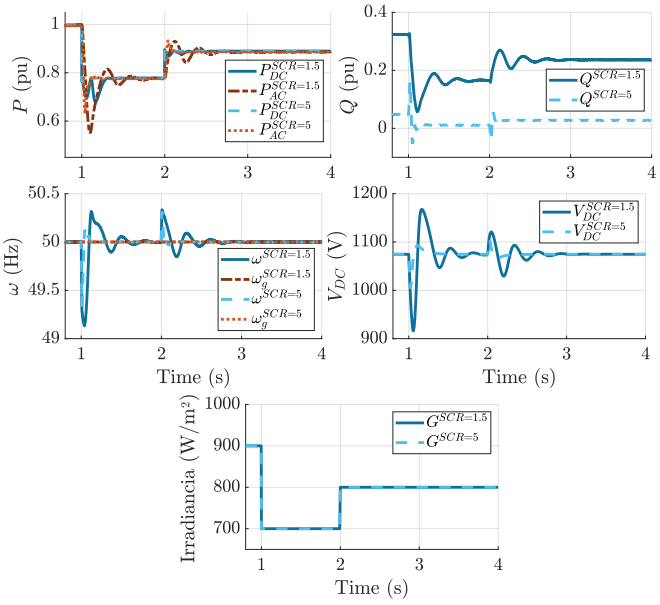

Fig. 12. Irradiation step performance of the control proposed operating in MPPT mode.

be implemented with the presented synchronization control. Moreover, in this operation mode, no power reserve or virtual inertia will be provided. However, the power plant operating in GFor will still be capable of providing voltage support and stability to the AC network.

V. Conclusion

The GFor control presented is capable of operating the central PV power plant, maintaining the DC voltage under control, even during relevant events. Moreover, it is capable of providing voltage support and stability to the grid. Further, it is suited to apply the MPPT and operate with reserve. Also,

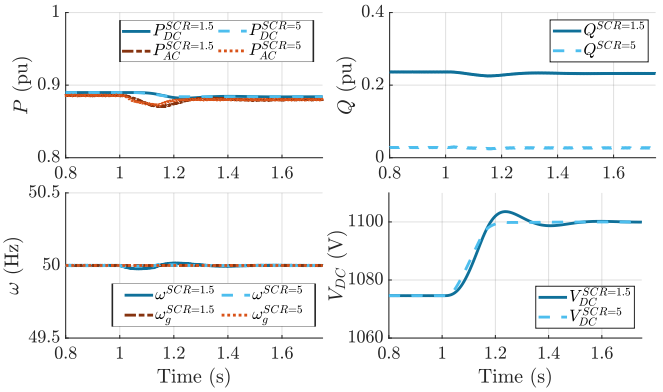

Fig. 13. Voltage reference jump performance of the control proposed.

it accomplishes the grid-code requirements during the faults. The advantages and limitations of the GFor control presented are the following:

A. Limitations

- The power reserve the converter can provide is limited by the power available. Then, it does not always provide a sufficient power reserve.
- The virtual inertia emulated depends on the capacitor size, which is usually small (0.02 s).
- If the control is operated at MPPT mode, the power that can be provided during an event is highly limited since the converter is already injecting its maximum power available and no storage is available.

B. Advantages

- The proposed control is capable of providing voltage support and stability operating in GFor with reserve and at MPPT. Moreover, the transition between operations is smooth.
- It is capable of using MPPT control from grid-forming schemes in a GFor control.
- It does not require a PLL to operate.
- It controls the DC voltage at the same time that it operates in GFor.
- The control can withstand AC events and resource limitations events, as demonstrated in Section IV.

In conclusion, the control presented has several limitations, mainly in the power it can provide in certain cases. However, it is essential to remark that these limitations are intrinsic to a PV power plant topology. Nevertheless, note that it provides constant support and stability to the AC voltage in the different operations. Furthermore, be aware that the GFor structure proposed provides frequency and voltage support, even the central or single-stage PV topology limitations. Ultimately, the proposed control is a viable and stable GFor control for a central PV power plant topology. Finally, this control will be capable of increasing the penetration of renewable sources into the grid and increasing its stability.

ACKNOWLEDGMENT

This work was supported by the European Union's Horizon 2020 Research and Innovation Programme [Powering System Flexibility in the Future through Renewable Energy Sources (POSYTYF) Project] under Grant 883985. This work also has been supported by the European Union's Next Generation PRTR program (FAIR project), with reference TED2021-129796B-C22. The work of Oriol Gomis-Bellmunt was supported by the Institució Catalana de Recerca i Estudis Avançats (ICREA) Academia Program. Eduardo Prieto-Araujo is a member of the Serra Húnter Programme. The work of Jaume Girona Badia was supported by FI-SDUR grant from AGAUR.

REFERENCES

[1] *Completing the map Power system needs in 2030 and 2040*. ENTSOE, 2021.

[2] VDE, "FNN Guideline: Grid forming behaviour of HVDC systems and DC-connected PPMs," https://shop.vde.com/en/fnn-guideline-hvdc-systems-2, Berlin, 2020.

[3] "D3.2 - overall specifications of the demonstrations," Apr 2022. [Online]. Available: https://www.osmose-h2020.eu/download/d3-2-overall-specifications-of-the-demonstrations/

[4] Y. Lin, J. H. Eto, B. B. Johnson, J. D. Flicker, R. H. Lasseter, H. N. Villegas Pico, G.-S. Seo, B. J. Pierre, and A. Ellis, "Research roadmap on grid-forming inverters," Nov 2020. [Online]. Available: https://www.osti.gov/biblio/1721727

[5] J. Girona-Badia, V. A. Lacerda, E. Prieto-Araujo, and O. Gomis-Bellmunt, "Limitations on the virtual inertia provision from grid-forming-connected renewable energy sources," in *19th International Conference on AC and DC Power Transmission (ACDC 2023)*, vol. 2023, 2023, pp. 166–173.

[6] A. L. Kumar, S. A. Alexander, and M. Rajendran, *Power electronic converters for solar photovoltaic systems*. Academic Press, 2020.

[7] A. Cabrera-Tobar, E. Bullich-Massagué, M. Aragüés-Peñalba, and O. Gomis-Bellmunt, "Topologies for large scale photovoltaic power plants," *Renewable and Sustainable Energy Reviews*, vol. 59, pp. 309–319, 2016. [Online]. Available: https://www.sciencedirect.com/science/article/pii/S1364032116000289

[8] R. Dogga and M. Pathak, "Recent trends in solar pv inverter topologies," *Solar Energy*, vol. 183, pp. 57–73, 2019. [Online]. Available: https://www.sciencedirect.com/science/article/pii/S0038092X19301999

[9] Z. Zeng, H. Yang, R. Zhao, and C. Cheng, "Topologies and control strategies of multi-functional grid-connected inverters for power quality enhancement: A comprehensive review," *Renewable and Sustainable Energy Reviews*, vol. 24, pp. 223–270, 2013. [Online]. Available: https://www.sciencedirect.com/science/article/pii/S1364032113001925

[10] L. Hassaine, E. OLias, J. Quintero, and V. Salas, "Overview of power inverter topologies and control structures for grid connected photovoltaic systems," *Renewable and Sustainable Energy Reviews*, vol. 30, pp. 796–807, 2014. [Online]. Available: https://www.sciencedirect.com/science/article/pii/S1364032113007545

[11] B. Pawar, E. I. Batzelis, S. Chakrabarti, and B. C. Pal, "Grid-forming control for solar pv systems with power reserves," *IEEE Transactions on Sustainable Energy*, vol. 12, no. 4, pp. 1947–1959, 2021.

[12] S. Nogami, A. Yokoyama, T. Daibu, and Y. Hono, "Virtual synchronous generator model control of pv for improving transient stability and damping in a large-scale power system," *Electrical Engineering in Japan*, vol. 208, no. 3-4, pp. 21–28, 2019.

[13] Z. Chen, D. Pattabiraman, R. H. Lasseter, and T. M. Jahns, "Certs microgrids with photovoltaic microsources and feeder flow control," in *2016 IEEE Energy Conversion Congress and Exposition (ECCE)*, 2016, pp. 1–8.

[14] I. Cvetkovic, D. Boroyevich, R. Burgos, C. Li, and P. Mattavelli, "Modeling and control of grid-connected voltage-source converters emulating isotropic and anisotropic synchronous machines," in *2015 IEEE 16th Workshop on Control and Modeling for Power Electronics (COMPEL)*, 2015, pp. 1–5.

[15] I. Ray and L. M. Tolbert, "Grid-forming inverter control design for pv sources considering dc-link dynamics," *IET Renewable Power Generation*, 2022.

[16] R. H. Lasseter, Z. Chen, and D. Pattabiraman, "Grid-forming inverters: A critical asset for the power grid," *IEEE Journal of Emerging and Selected Topics in Power Electronics*, vol. 8, no. 2, pp. 925–935, 2020.

[17] O. Gomis-Bellmunt and A. Junyent-Ferré, "Control of doubly fed induction generators under balanced and unbalanced voltage conditions," in *Handbook Of Renewable Energy Technology*. World Scientific, 2011, pp. 757–783.

[18] S. Dadjo Tavakoli, E. Prieto-Araujo, O. Gomis-Bellmunt, and S. Galceran-Arellano, "Fault ride-through control based on voltage prioritization for grid-forming converters," *IET Renewable Power Generation*, vol. 17, no. 6, pp. 1370–1384, 2023.

[19] J. A. Suul, S. D'Arco, and G. Guidi, "A single-phase virtual synchronous machine for providing vehicle-to-grid services from electric vehicle battery chargers," in *Proceedings of the International Electric Vehicle Technology Conference & Automotive Power Electronics*, 2014, p. 7.

[20] J. A. Suul, S. D'Arco, and G. Guidi, "Virtual synchronous machine-based control of a single-phase bi-directional battery charger for providing vehicle-to-grid services," *IEEE Transactions on Industry Applications*, vol. 52, no. 4, pp. 3234–3244, 2016.

[21] J. Freytes, A. Rossé, V. Costan, and G. Prime, "Grid-forming control based on emulated synchronous condenser strategy compliant with challenging grid code requirements," *arXiv preprint arXiv:2303.00391*, 2023.

[22] O. Mo, S. D'Arco, and J. A. Suul, "Evaluation of virtual synchronous machines with dynamic or quasi-stationary machine models," *IEEE Transactions on industrial Electronics*, vol. 64, no. 7, pp. 5952–5962, 2016.

[23] E. Prieto-Araujo, A. Egea-Alvarez, S. Fekriasl, and O. Gomis-Bellmunt, "DC voltage droop control design for multiterminal HVDC systems considering AC and DC grid dynamics," *IEEE Transactions on Power Systems*, vol. 31, no. 2, pp. 575–585, April 2016.

[24] A. Yepes, A. Vidal, O. Lopez, and J. Doval-Gandoy, "Evaluation of techniques for cross-coupling decoupling between orthogonal axes in double synchronous reference frame current control," *IEEE Transactions on Industrial Electronics*, vol. 61, pp. 3527–3531, 07 2014.

[25] J. Girona-Badia, E. Prieto-Araujo, and O. Gomis-Bellmunt, "Pairing grid-forming vsc filter topologies with voltage control structures," *International Journal of Electrical Power & Energy Systems*, vol. 155, p. 109670, 2024. [Online]. Available: https://www.sciencedirect.com/science/article/pii/S0142061523007275

[26] P. Electronics. (2024) Solar brochure. [Online]. Available: https://power-electronics.com/en/solar/hem

[27] A. Egea-Alvarez, A. Junyent-Ferré, and O. Gomis-Bellmunt, "Active and reactive power control of grid connected distributed generation systems," in *Modeling and Control of Sustainable Power Systems: Towards Smarter and Greener Electric Grids*. Springer, 2012, pp. 47–81.

[28] M. G. Villalva, J. R. Gazoli, and E. Ruppert Filho, "Comprehensive approach to modeling and simulation of photovoltaic arrays," *IEEE Transactions on power electronics*, vol. 24, no. 5, pp. 1198–1208, 2009.

[29] C. Carrero, J. Amador, and S. Arnaltes, "A single procedure for helping pv designers to select silicon pv modules and evaluate the loss resistances," *Renewable energy*, vol. 32, no. 15, pp. 2579–2589, 2007.

[30] E. Commission, "Commission regulation (eu) 2016/631 of 14 april 2016, establishing a network code on requirements for grid connection of generators," *Off. J. Eur. Union*, 2016.